Diagn Interv Radiol 2026; DOI: 10.4274/dir.2026.263712

ABDOMINAL IMAGING

ORIGINAL ARTICLE

Dual-layer spectral detector computed tomography of peritumoral fat for preoperative prediction of tumor budding in colorectal adenocarcinoma

Jian-Bo Xu[1,#]
Wei-Jin Zhong[1,#]
Yuan-Hui Li[1,#]
Xiang Zhou[1]
Su-E Cao[1]
Xiao-Min Liu[2]
Ruo-Mi Guo[1]

[1]The Third Affiliated Hospital, Sun Yat-Sen University, Department of Radiology, Guangzhou, China

[2]Philips Healthcare, Clinical and Technical Support, Guangzhou, China

#Contributed equally to this work as the first authors.

Corresponding author: Ruo-Mi Guo

E-mail: guoruomi86@mail.sysu.edu.cn

Received 25 October 2025; revision requested 01 December 2025; accepted 25 January 2026.

Epub: 06.03.2026

Publication date:

DOI: 10.4274/dir.2026.263712

PURPOSE

To explore the value of dual-layer spectral detector computed tomography (DLSCT)-derived parameters from peritumoral fat for preoperative tumor budding (TB) grade assessment in patients with colorectal adenocarcinoma (CRAC).

METHODS

This retrospective study enrolled 90 patients with pathologically confirmed CRAC who underwent preoperative DLSCT between February 2024 and July 2025. Patients were stratified into low-grade and intermediate- to high-grade TB groups based on histopathology. The effective atomic number (Z_{eff}), iodine concentration (IC), normalized IC concentration (NIC), virtual monoenergetic images (VMIs) at 40, 50, 60, and 70 keV in arterial phase (AP) and venous phase (VP), and the arterial enhancement fraction of intratumor and peritumoral fat were measured. Independent predictors were identified via multivariable logistic regression, and diagnostic performance was evaluated using receiver operating characteristic analysis.

RESULTS

Multiple DLSCT-derived parameters of the peritumoral fat, including VMIs (40–70 keV) and Z_{eff} in both AP and VP, as well as NIC in VP, were significantly higher in the intermediate- to high-TB group than in the low-TB group (all $P < 0.05$; AP-VMI 40 keV, $P = 0.001$; AP-VMI 50 keV, $P = 0.002$; AP-VMI 60 keV, $P = 0.001$; AP-VMI 70 keV, $P = 0.001$; AP-Z_{eff}, $P = 0.002$; VP-VMI 40 keV, $P = 0.004$; VP-VMI 50 keV, $P = 0.001$; VP-VMI 60 keV, $P = 0.001$; VP-VMI 70 keV, $P < 0.001$; VP-VMI 70 keV, $P < 0.001$; VP-NIC, $P = 0.024$; VP-Z_{eff}, $P = 0.019$), whereas other parameters derived from DLSCT were not significantly different between these two groups ($P > 0.05$). Multivariable analysis revealed that VMIs (40–70 keV) and Z_{eff} in both AP and VP, as well as NIC in VP, remained independent predictors of TB grade. Among these, VMI at 70 keV in VP exhibited the strongest discriminatory ability [area under the curve (AUC): 0.742, 95% confidence interval (CI): 0.623–0.860]. The combined model integrating these parameters yielded the best predictive performance (AUC: 0.809, 95% CI: 0.713–0.906).

CONCLUSION

DLSCT -derived quantitative parameters of peritumoral fat, particularly VMI and Z_{eff} values from both AP and VP, serve as independent predictors of TB grade in CRAC.

CLINICAL SIGNIFICANCE

DLSCT-derived quantitative parameters of peritumoral fat can serve as a complementary, noninvasive quantitative imaging biomarker for preoperatively predicting TB grade in CRAC.

KEYWORDS

Colorectal adenocarcinoma, tumor budding, peritumoral fat, dual-layer spectral detector computed tomography

You may cite this article as: Xu JB, Zhong WJ, Li YH, et al. Dual-layer spectral detector computed tomography of peritumoral fat for preoperative prediction of tumor budding in colorectal adenocarcinoma. *Diagn Interv Radiol*. 06 March 2026 DOI: 10.4274/dir.2026.263712 [Epub Ahead of Print].

Colorectal cancer (CRC) ranks as the third most common cancer worldwide and the second leading cause of cancer-related deaths.[1,2] Tumor budding (TB) is recognized as a significant prognostic factor in colorectal adenocarcinoma (CRAC) by the National Comprehensive Cancer Network and European Society for Medical Oncology guidelines.[3] Defined by single cells or small clusters of up to four cells at the invasive tumor front, TB is a robust independent prognostic marker.[4] It stratifies patients into risk categories for recurrence and mortality,[5] making its preoperative identification crucial for treatment planning. Although histopathological biopsy remains the gold standard for TB grading, the technique is invasive and carries potential complications.[4] Contrast-enhanced computed tomography (CECT) is a cornerstone in CRAC management, providing standardized protocols for initial staging and therapy monitoring.[6,7] However, CECT is often insufficient for the comprehensive preoperative prediction of CRC pathological types, necessitating the development of more advanced quantitative imaging techniques.[8]

Dual-layer spectral detector CT (DLSCT) is an advanced modality that generates material decomposition images, such as iodine- or water-based maps. With more quantitative parameters than CECT, DLSCT has proven useful in diagnosing and managing various tumors.[6,9-11] It demonstrates advantages in T-staging, evaluating tumor differentiation, perineural invasion (PNI), and lymphovascular invasion in CRC,[12-17] and has been applied to assess TB grade.[17] Additionally, DLSCT-based radiomics and machine learning have been used to evaluate distant metastasis and microsatellite instability in CRC.[18,19]

In precision oncology, the peritumoral fat microenvironment (PFME) is increasingly recognized as a prognostic marker. Quantitative PFME analysis can predict histopathological markers and molecular subtypes. The mesenchymal transition of peritumoral adipose tissue is characterized by the generation of dedifferentiated adipocytes, which constitute the major stromal cell type within tumors.[20-22] A dynamic interaction exists between tumors and adipose tissue, where cancer cells induce metabolic reprogramming in adjacent adipocytes to promote progression.[23] CRC remodels the peritumoral fat through an initial phase of structural disruption followed by reorganization, ultimately leading to a brown fat-like phenotype.[24] These alterations directly modulate X-ray attenuation properties, which are quantified by DLSCT, providing a direct mechanistic link between spectral parameters of peritumoral fat and TB, a histopathological marker of local tumor invasiveness.[17]

However, the quantitative application of DLSCT for peritumoral fat assessment in CRAC TB grading has not been previously explored. Therefore, this study evaluates the utility of DLSCT quantitative parameters for the preoperative diagnosis of TB grade in patients with CRAC.

Main points

- Dual-layer spectral detector computed tomography-derived quantitative parameters of intratumor and peritumoral fat are used for assessing tumor budding (TB) grade in colorectal adenocarcinoma (CRAC).
- The virtual monoenergetic images (VMIs) (40–70 keV) and effective atomic number (Z_{eff}) in both arterial phase (AP) and venous phase (VP), as well as normalized iodine concentration in the VP of peritumoral fat, were higher in the intermediate- to high-TB group than in the low-TB group.
- The VMI and Z_{eff} values from both the AP and the VP of peritumoral fat serve as independent predictors of TB grade in CRAC.

Methods

Patients

This study was approved by the Institutional Research Ethics Committee of the Third Affiliated Hospital of Sun Yat-Sen University (clinical trial number: II2025-229-01, date: 06.17.2025), and the requirement for informed consent was waived by the ethics committee due to the retrospective nature of the study. Between February 2024 and July 2025, 577 consecutive patients with pathologically confirmed CRAC who underwent preoperative spectral CT were initially enrolled. The inclusion criteria were (1) spectral CT performed within 2 weeks before surgery and (2) no prior treatment. The exclusion criteria included (1) preoperative radiotherapy or chemotherapy (n = 446), (2) CT-surgery interval exceeding 2 weeks (n = 20), (3) poor image quality due to artifacts (n = 8), and (4) mucinous or signet ring cell carcinoma (n = 13). The final cohort comprised 90 patients (24 with intermediate- to high-grade TB; 66 with low-grade TB). The entire analytical workflow of the study and the patient selection process are detailed in Figures 1 and 2, respectively.

Image acquisition

All scans were performed using a spectral CT scanner (IQon Spectral CT, Philips Healthcare, Best, The Netherlands). Patients were scanned in the supine position from the diaphragm to the pubic symphysis. The key parameters were as follows: tube voltage: 120 kV, automatic tube current modulation, pitch: 0.99, rotation time: 0.75 s, detector configuration: 64 × 0.625 mm, and slice thickness: 1.25 mm. The arterial phase (AP) was triggered at 150 Hounsfield units (HU) in the abdominal aorta, followed by a venous phase (VP) 60 seconds later.

Non-ionic contrast (iodixanol, Visipaque™, 300 mg I/mL) was administered intravenously at 1.2 mL/kg via a high-pressure syringe (3.0 mL/s), followed by a 30-mL saline flush (3.0 mL/s).

Image evaluation

Images were analyzed on an IntelliSpace Portal (Philips Healthcare) using Spectral CT Viewer software. Two radiologists (10 and 5 years of experience, respectively), blinded to

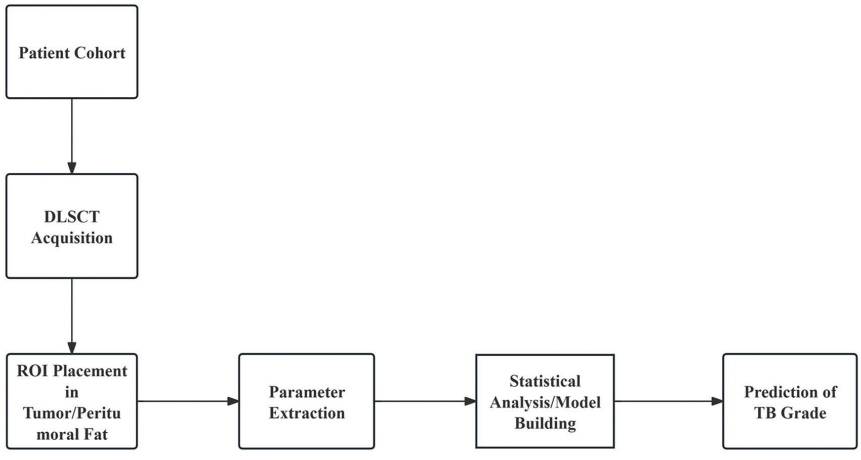

Figure 1. The entire analytical workflow of the study. DLSCT: dual-layer spectral detector computed tomography; TB: tumor budding; ROI, region of interest.

the pathological results, adhered to the same standardized protocol and independently established regions of interest (ROIs). Intratumor ROIs were drawn on 70-keV virtual monoenergetic image (VMI) slices showing the largest tumor area, avoiding necrosis, vessels, and cysts. Peritumoral fat ROIs were established, with a width of ≤ 5 and a 1-mm margin from the tumor (mean: 5.5 mm^2, range: 2.0–12.5 mm^2).[25]

The quantitative parameters, including iodine concentration (IC) for both the tumor and the abdominal aorta or iliac vessels, effective atomic number (Z_{eff}), and VMIs at 40, 50, 60, and 70 keV, were generated. All measurements were performed independently by two blinded radiologists, and the mean values were used for final analysis. Normalized IC (NIC) was calculated to standardize measurements.

Pathological evaluation

Grading of TB was conducted using hematoxylin–eosin staining, assessed by two gastrointestinal pathologists (10 and 20 years' experience, respectively) following International Tumor Budding Consensus Conference 2016 guidelines.[26] Disagreements were resolved by consensus. Buds were counted at 20 × magnification and normalized to buds/0.785 mm^2.[26] The grading was as follows: Bd1 (low, ≤ 4 buds), Bd2 (intermediate, 5–9 buds), and Bd3 (high, ≥ 10 buds). For the analysis, Bd1 was classified as low-grade TB, and Bd2 and Bd3 as intermediate- to high-grade TB.

Statistical analysis

All statistical analyses were performed using SPSS (version 26.0; IBM Corp., Chicago, IL, USA) and GraphPad Prism (version 9.5.1; GraphPad Software, San Diego, CA, USA). Data normality was assessed using the Shapiro–Wilk test. Normally distributed variables are presented as mean ± standard deviation, and non-normally distributed variables are presented as median and interquartile range. Group comparisons were conducted using the Mann–Whitney U test. Univariable and multivariable logistic regression analyses were performed to calculate odds ratios (ORs) with corresponding 95% confidence intervals (CIs). Predictive performance was evaluated using the area under the receiver operating characteristic curve (AUC), and AUCs were compared using the DeLong test. Multicollinearity was assessed using variance inflation factors (VIFs); variables with VIF > 10 were excluded. A backward stepwise elimination method (likelihood ratio) with a removal criterion of $P > 0.05$ was used to derive the final model. Interobserver agreement was assessed using the intraclass correlation coefficient (ICC), which was classified as poor (0–0.20), fair (0.21–0.40), moderate (0.41–0.60), good (0.61–0.80), or excellent (0.81–1.00). A two-sided P value < 0.05 was considered statistically significant.

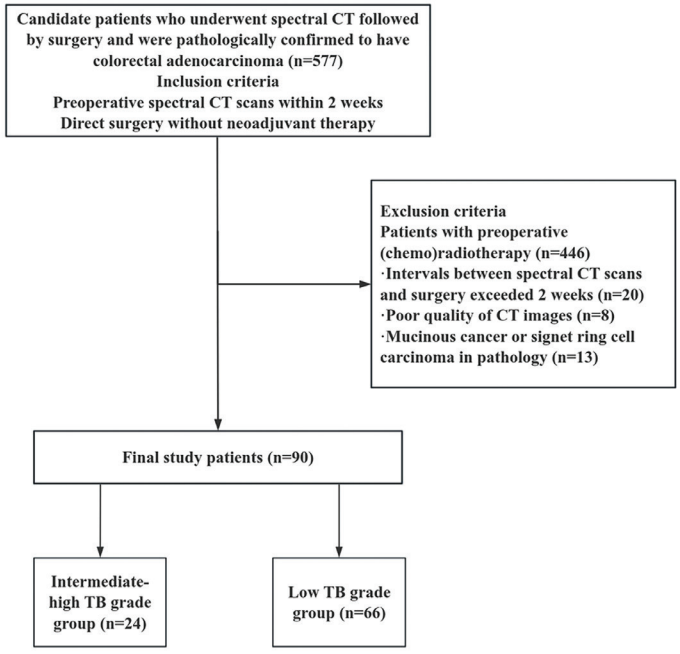

Figure 2. Patient screening flowchart. CT, computed tomography; CRAC, colorectal adenocarcinoma; TB: tumor budding.

Results

Demographic, clinical, and pathologic features

As shown in Table 1, 90 patients (53 men and 37 women; median age: 62 years) were enrolled in this study. All clinical characteristics (age, $P = 0.51$; gender, $P = 0.22$; location, $P = 0.75$; carcinoembryonic antigen, $P = 0.51$; carbohydrate antigen 199, $P = 0.26$) and

Table 1. Clinical characteristics of the patients with colorectal adenocarcinoma

Characteristics	Overall	Tumor budding		*P* value
	n = 90	Intermediate–high n = 24	Low n = 66	
Age (mean ± SD)	61.61 ± 11.34	59.38 ± 10.45	62.42 ± 11.61	0.51
Gender				
Female	37 (41.11%)	6 (25.00%)	31(46.97%)	0.22
Male	53 (58.89%)	18 (75.00%)	35 (53.03%)	
Location				
Right	29 (32.22%)	9 (37.50%)	20 (30.30%)	0.75
Left	61 (67.78%)	15 (62.50%)	46 (69.70%)	
cT stage				
T1-2	17 (18.89%)	2 (8.33%)	15 (22.73%)	0.82
T3	50 (55.56%)	18 (75.00%)	32 (48.48%)	
T4	23 (25.55%)	4 (16.67%)	19 (28.79%)	
cN stage				
N0	47 (52.22%)	10 (41.67%)	37 (56.06%)	0.51
N1	28 (31.11%)	10 (41.67%)	18 (27.27%)	
N2	15 (16.67%)	4 (16.66%)	11 (16.67%)	

qualitative parameters of CECT (cT stage, P = 0.82; cN stage, P = 0.51; c-extramural vascular invasion, P = 0.24) were not significantly different between low-grade TB and intermediate- to high-grade TB of CRAC (P > 0.05).

Among the spectral parameters, VMIs (40–70 keV) and Z_{eff} in both AP and VP, as well as NIC in the VP of peritumoral fat, were significantly different between low-grade TB and intermediate- to high-grade TB of CRAC (all P < 0.05; AP-VMI 40 keV, P = 0.001; AP-VMI 50 keV, P = 0.002; AP-VMI 60 keV, P = 0.001; AP-VMI 70 keV, P = 0.001; AP-Z_{eff}, P = 0.002; VP-VMI 40 keV, P = 0.004; VP-VMI 50 keV, P = 0.001; VP-VMI 60 keV, P = 0.001; VP-VMI 70 keV, P < 0.001; VP-NIC, P = 0.024; VP-Z_{eff}, P = 0.019) (Table 2). Examples of CRAC cases with low-grade TB and intermediate- to high-grade TB are shown in Figures 3 and 4.

Spectral computed tomography parameters, predictors, and logistic models for tumor budding prediction

As shown in Table 3, univariate analysis showed that VMIs at 40, 50, 60, and 70 keV, Z_{eff} in both AP and VP, and NIC in the VP of peritumoral fat were associated with the TB of CRAC (P < 0.05; AP-VMI 40 keV, P = 0.001; AP-VMI 50 keV, P = 0.002; AP-VMI 60 keV, P = 0.002; AP-VMI 70 keV, P = 0.001; AP-Z_{eff}, P = 0.002; VP-VMI 40 keV, P = 0.004; VP-VMI 50 keV, P = 0.001; VP-VMI 60 keV, P = 0.001; VP-VMI 70 keV, P < 0.001; VP-NIC, P = 0.024; VP-Z_{eff}, P = 0.019). In the multivariate analysis, VMI at 40, 50, 60, and 70 keV, and Z_{eff} in both AP and VP remained independent predictors of TB grade (OR: 1.025, 95% CI: 0.610–0.833, P = 0.001; OR: 0.987, 95% CI: 0.601–0.827, P = 0.002; OR: 0.845, 95% CI: 0.606–0.830, P = 0.002; OR: 1.166, 95% CI: 0.609–0.832, P = 0.002; OR: 8.649, 95% CI: 0.594–0.826, P = 0.002; OR: 0.910, 95% CI: 0.575–0.820, P = 0.004; OR: 1.091, 95% CI: 0.608–0.841, P = 0.001; OR: 1.069, 95% CI: 0.604–0.841, P = 0.001; OR: 1.015, 95% CI: 0.623–0.860, P = 0.001; OR: 0.433, 95% CI: 0.533–0.792, P = 0.019). The AUCs of the spectral CT parameters are presented in Table 4, ranging from 0.662 to 0.742. Among these, VP-VMI at 70 keV of peritumoral fat yielded the highest AUC of 0.742, with sensitivities of 66.67% and specificities of 81.82% for differentiating between low-grade and intermediate- to high-grade TB. Combining all spectral parameters and clinical characteristics further improved predictive ability, with an AUC of 0.809, a sensitivity of 70.80%, and a specificity of 81.80% (Figures 5 and 6, Table 4). Figure 7 presents the results from the final fitted multivariable logistic regression model.

Table 1. Continued

Characteristics	Overall	Tumor budding		*P* value
	n = 90	Intermediate–high n = 24	Low n = 66	
cEMVI				
Positive (+)	26 (28.89%)	10 (41.67%)	16 (24.24%)	0.24
Negative (–)	64 (71.11%)	14 (58.33%)	50 (75.76%)	
CEA				
< 5 ng/mL	62 (68.89%)	15 (62.50%)	47 (71.21%)	0.51
≥ 5 ng/mL	28 (31.11%)	9 (37.50%)	19 (28.79%)	
CA199				
< 35 U/mL	78 (86.67%)	19 (79.17%)	59 (89.39%)	0.26
≥ 35 U/mL	12 (13.33%)	5 (20.83%)	7 (10.61%)	

SD, standard deviation; cT stage, clinical T stage based on computed tomography; cN stage, clinical N stage based on computed tomography; cEMVI, extramural vascular invasion based on computed tomography; CEA, carcinoembryonic antigen; CA199, carbohydrate antigen 199.

Table 2. Quantitative parameters of DLSCT in the evaluation of tumor budding grade in patients with colorectal adenocarcinoma

Parameters	Overall	Tumor budding		*P* value
	n = 90	Intermediate– high n = 24	Low n = 66	
Intratumor				
AP-VMI 40 keV	171.70 ± 51.51	162.80 ± 50.94	175.00 ± 51.73	0.194
AP-VMI 50 keV	121.10 ± 32.68	117.10 ± 29.53	122.60 ± 25.16	0.297
AP-VMI 60 keV	96.79 ± 23.36	94.17 ± 20.91	97.74 ± 24.26	0.387
AP-VMI 70 keV	85.03 ± 18.00	83.47 ± 17.72	85.59 ± 18.21	0.423
AP-IC	1.45 ± 0.57	1.32 ± 0.58	1.50 ± 0.57	0.135
AP-NIC	0.15 ± 0.06	0.14 ± 0.07	0.15 ± 0.62	0.124
AP-Z_{eff}	8.09 ± 0.29	8.02 ± 0.30	8.12 ± 0.29	0.151
VP-VMI 40 keV	169.30 ± 35.87	167.80 ± 37.87	169.90 ± 35.40	0.777
VP-VMI 50 keV	121.40 ± 24.52	122.10 ± 23.15	121.20 ± 25.16	0.991
VP-VMI 60 keV	96.05 ± 17.66	96.83 ± 16.29	95.77 ± 18.25	0.944
VP-VMI 70 keV	83.70 ± 13.77	83.72 ± 13.69	83.70 ± 13.90	0.995
VP-IC	1.43 ± 0.37	1.41 ± 0.41	1.44 ± 0.36	0.801
VP-NIC	0.34 ± 0.09	0.35 ± 0.09	0.33 ± 0.09	0.588
VP-Z_{eff}	8.10 ± 0.22	8.06 ± 0.28	8.11 ± 0.19	0.767
AEF	1.22 ± 1.32	1.18 ± 0.35	1.23 ± 1.53	0.107
Peritumoral fat				
AP-VMI 40 keV	−43.39 ± 56.42	−11.00 ± 46.51	−55.17 ± 55.36	0.001*
AP-VMI 50 keV	−36.19 ± 43.25	−12.14 ± 36.57	−44.93 ± 42.39	0.002*
AP-VMI 60 keV	−31.73 ± 35.71	−12.34 ± 30.88	−38.78 ± 34.92	0.001*
AP-VMI 70 keV	−29.72 ± 30.82	−12.33 ± 27.71	−36.04 ± 29.61	0.001*
AP-IC	0.26 ± 0.28	0.30 ± 0.22	0.25 ± 0.30	0.083
AP-NIC	0.03 ± 0.03	0.31 ± 0.20	0.02 ± 0.03	0.054
AP-Z_{eff}	6.98 ± 0.40	7.20 ± 0.31	6.90 ± 0.40	0.002*
VP-VMI 40 keV	−30.23 ± 54.07	−2.79 ± 49.04	−40.21 ± 52.66	0.004*
VP-VMI 50 keV	−28.24 ± 42.84	−4.10 ± 35.48	−37.01 ± 42.12	0.001*
VP-VMI 60 keV	−25.41 ± 34.34	−6.04 ± 29.38	−32.45 ± 33.46	0.001*
VP-VMI 70 keV	−23.15 ± 29.99	−5.68 ± 25.63	−29.50 ± 29.08	<0.001*
VP-IC	0.26 ± 0.22	0.33 ± 0.24	0.24 ± 0.21	0.083

Interobserver agreement

The interobserver agreement for CT images measured by two radiologists was excellent, with ICC values ranging from 0.657 (95% CI: 0.479–0.774) to 0.944 (95% CI: 0.914–0.963), except for the arterial enhancement fraction of peritumoral fat (Supplementary Table 1). This may be attributed to increased image noise at low keV or the challenge of consistently placing ROIs in heterogeneous peritumoral fat.

Table 2. Continued

Parameters	Overall	Tumor budding		*P* value
	n = 90	Intermediate– high n = 24	Low n = 66	
VP-NIC	0.61 ± 0.50	0.08 ± 0.06	0.05 ± 0.05	0.024*
VP-Z_{eff}	7.08 ± 0.39	7.23 ± 0.37	7.03 ± 0.38	0.019*
AEF	1.98 ± 3.29	1.25 ± 1.14	2.26 ± 3.80	0.436

*Independently significant variables. Values are presented as mean ± standard deviation. DLSCT: dual-layer spectral detector computed tomography; VMI: virtual monoenergetic image; Z_{eff}: effective atomic number; IC: iodine concentration; NIC: normalized iodine concentration; AEF: arterial enhancement fraction; AP, arterial phase; VP, venous phase.

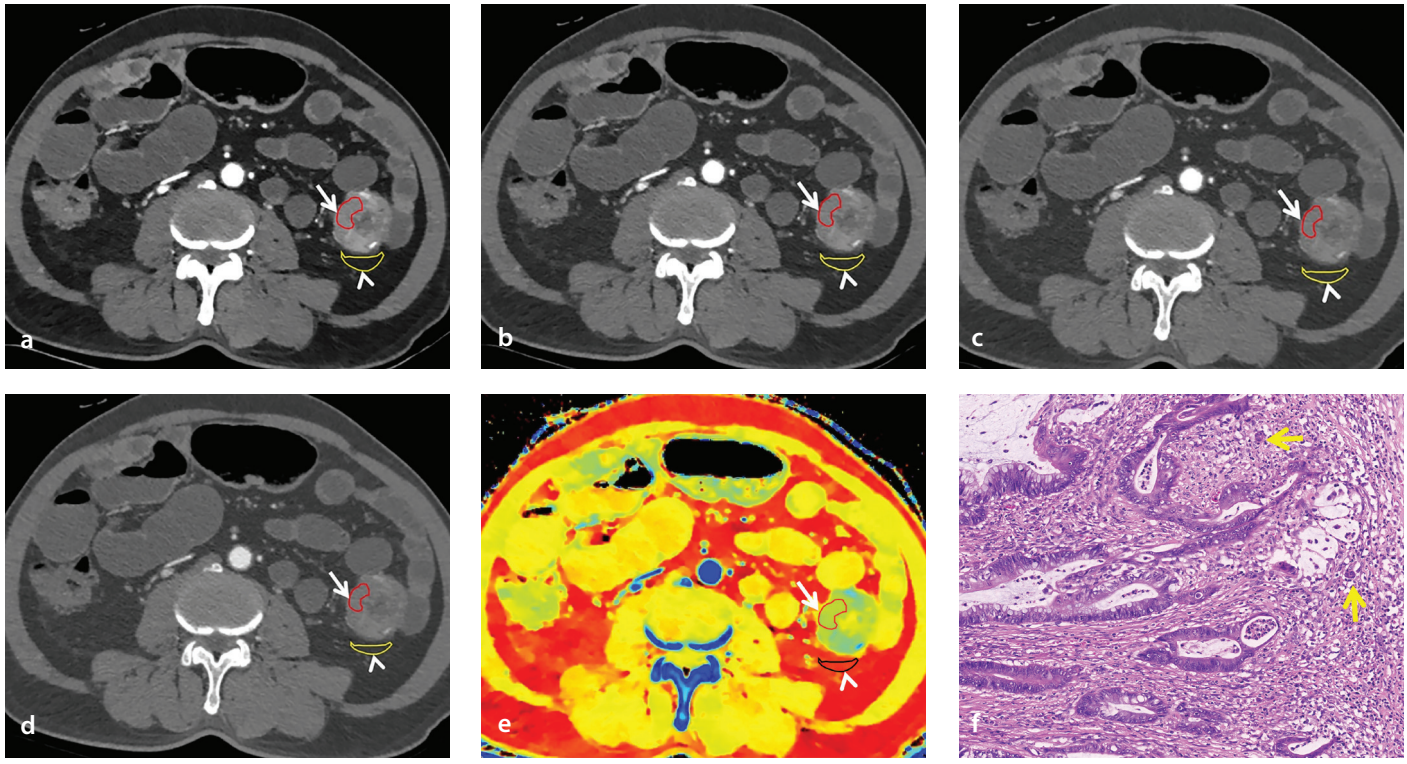

Figure 3. A 68-year-old man with low-grade TB descending colon adenocarcinoma. Regions of interest were established on the tumor (red) and peritumoral fat (yellow). **(a)** 40 keV-AP: tumor 133.05 HU (arrow), fat –147.15 HU (arrowhead); **(b)** 50 keV-AP: tumor 93.3 HU (arrow), fat –114.45 HU (arrowhead); **(c)** 60 keV-AP: tumor 75.9 HU (arrow), fat –95.3 HU (arrowhead); **(d)** 70 keV-AP: tumor 71.0 HU (arrow), fat –83.85 HU (arrowhead); **(e)** AP-Z_{eff}: tumor 7.91 (arrow), fat 6.21 (arrowhead); **(f)** histopathology shows < 5 buds (arrow) (hematoxylin–eosin, × 200). TB, tumor budding; HU, Hounsfield unit; AP, arterial phase; VP, venous phase.

Table 3. Univariate and multivariate analysis of predictors of tumor budding grade in patients with colorectal adenocarcinoma

Parameters	Univariate parameter		Multivariate parameter	
	Z/χ^2	*P* value	OR	*P* value
Age	–1.196	0.232		
Gender	–1.889	0.062		
cEMVI	–1.618	0.109		
cT stage	0.295	0.768		
cN stage	–0.799	0.426		
CEA	0.958	0.338		
CA199	1.481	0.139		
Intratumor				
AP-VMI 40 keV	–1.305	0.192		
AP-VMI 50 keV	–1.049	0.294		
AP-VMI 60 keV	–0.871	0.384		
AP-VMI 70 keV	–0.808	0.419		

Table 3. Continued

Parameters	Univariate parameter		Multivariate parameter	
	Z/χ^2	*P* value	OR	*P* value
VP-Z_{eff}	−0.301	0.763		
AEF	1.615	0.106		
AP-IC	−1.501	0.133		
AP-NIC	−1.542	0.123		
AP-Z_{eff}	−1.442	0.149		
VP-VMI 40 keV	−0.287	0.774		
VP-VMI 50 keV	0.014	0.989		
VP-VMI 60 keV	0.073	0.942		
VP-VMI 70 keV	−0.009	0.993		
VP-IC	−0.255	0.798		
VP-NIC	0.547	0.584		
Peritumoral fat				
AP-VMI 40 keV	3.198	0.001*	1.026	0.001**
AP-VMI 50 keV	3.089	0.002*	0.990	0.002**
AP-VMI 60 keV	3.148	0.002*	0.849	0.002**
AP-VMI 70 keV	3.184	0.001*	1.157	0.002**
AP-IC	1.735	0.083		
AP-NIC	1.926	0.054		
AP-Z_{eff}	3.034	0.002*	6.811	0.002**
VP-VMI 40 keV	2.856	0.004*	0.913	0.004**
VP-VMI 50 keV	3.248	0.001*	1.091	0.001**
VP-VMI 60 keV	3.216	0.001*	1.062	0.001**
VP-VMI 70 keV	3.495	<0.001*	1.016	0.001**
VP-IC	1.738	0.082		
VP-NIC	2.249	0.024*	4.441	0.169
VP-Z_{eff}	2.345	0.019*	0.466	0.019**
AEF	−0.786	0.432		

*Variables included multivariable analysis based on $P < 0.1$; **Independently significant variables.
OR, odds ratio; cEMVI: extramural vascular invasion based on computed tomography; cT stage, clinical T stage based on computed tomography; cN stage, clinical N stage based on computed tomography; CEA, carcinoembryonic antigen; CA199, carbohydrate antigen199; PNI, perineural invasion; VMI, virtual monoenergetic image; Z_{eff}, effective atomic number; IC, iodine concentration; NIC, normalized iodine concentration; AEF, arterial enhancement fraction; VMI, virtual monoenergetic image; AP, arterial phase; VP, venous phase.

Table 4. Values of spectral parameters of peritumoral fat for evaluating the tumor budding grade in patients with colorectal adenocarcinoma

Parameter	AUC (95% CI)	Cut-off	Sensitivity	Specificity
AP-VMI 40 keV	0.721 (0.610, 0.833)	−37.43	79.17	57.58
AP-VMI 50 keV	0.714 (0.601, 0.827)	−41.85	79.17	54.55
AP-VMI 60 keV	0.718 (0.606, 0.830)	−48.63	91.67	43.94
AP-VMI 70 keV	0.720 (0.609, 0.832)	−40.90	87.50	50.00
AP- Z_{eff}	0.710 (0.594, 0.826)	6.86	91.67	45.45
VP-VMI 40 keV	0.698 (0.575, 0.820)	−12.53	66.67	71.21
VP-VMI 50 keV	0.725 (0.608, 0.841)	−4.30	62.50	80.30
VP-VMI 60 keV	0.723 (0.604, 0.841)	−3.55	62.50	81.82
VP-VMI 70 keV	0.742 (0.623, 0.860)	−5.10	66.67	81.82
VP-Z_{eff}	0.662 (0.533, 0.792)	7.19	66.67	69.70
All parameters combined	0.809 (0.713, 0.906)	0.38	70.80	81.80

*Independently significant variables. AUC, area under curve; CI, confidence intervals; VMI, virtual monoenergetic image; Z_{eff}, effective atomic number; VMI, virtual monoenergetic image; AP, arterial phase; VP, venous phase.

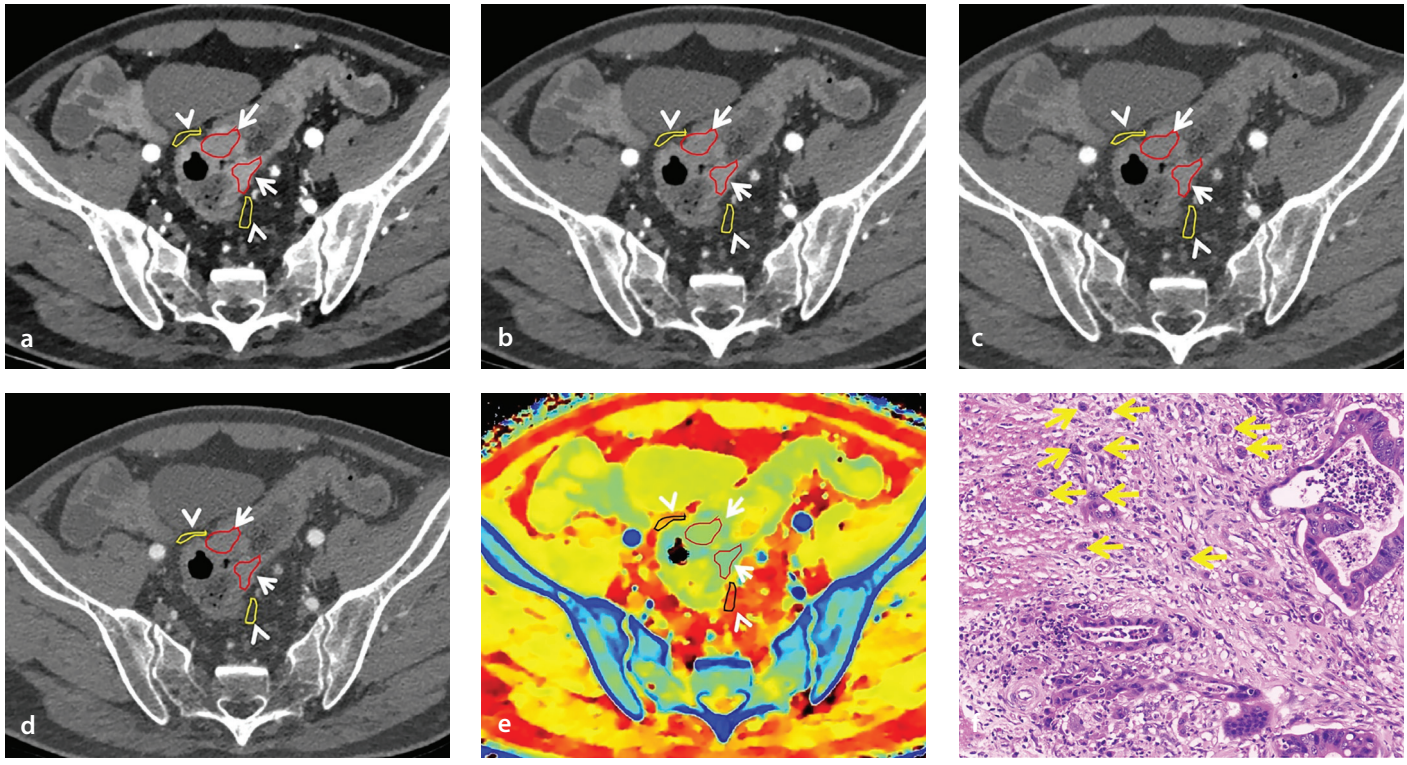

Figure 4. A 67-year-old man with high-grade-TB sigmoid colon adenocarcinoma. Regions of interest were established on the tumor (red) and peritumoral fat (yellow). **(a)** 40 keV-AP: tumor 162.85 HU (arrow), fat 22.45 HU (arrowhead); **(b)** 50 keV-AP: tumor 120.35 HU (arrow), fat 8.05 HU (arrowhead); **(c)** 60 keV-AP: tumor 95.4 HU (arrow), fat −0.4 HU (arrowhead); **(d)** 70 keV-AP: tumor 80.5 HU (arrow), fat −5.55 HU (arrowhead); **(e)** AP-Z_{eff}: tumor 8.09 (arrow), fat 7.44 (arrowhead); **(f)** histopathology shows > 10 buds (arrow) (HE, ×200). TB, tumor budding; HU, Hounsfield unit; AP, arterial phase; VP, venous phase.

Discussion

This study identified DLSCT-derived quantitative parameters of peritumoral fat—specifically AP and VP VMI and Z_{eff} values—as independent predictors of TB grade in CRAC. This predictive utility is likely mediated by a mesenchymal transition of the peritumoral fat, characterized by marked metabolic rewiring (e.g., upregulation of UCP-1, TMEM26, and PON3, and downregulation of Pref-1 and adiponectin), which generates dedifferentiated adipocytes that form a key stromal component within tumors.[20,27]

Multiparametric DLSCT—including VMIs, IC, Z_{eff}, and the HU curve slope (λHU) —provides valuable insights for tumor assessment.[28-30] Iodine mapping quantitatively evaluates microcirculation via IC, offering clinical value in CRAC for staging, differentiation, PNI, and lymph node metastasis assessment.[7,12,14,31] Low-energy 40-keV VMIs provide a superior signal-to-noise ratio and contrast-to-noise ratio, improving tumor detection clarity.[32,33] This enhancement stems from the proximity of 40 keV to the iodine K-edge (33 keV), optimizing visualization of iodine-rich areas.[33,34] Tumor vascularization, derived from intrinsic angiogenesis and co-option of host vessels,[35] correlates with growth and metastatic potential.[35,36] The Z_{eff} quantifies material composition by representing equivalent elemental atomic numbers in X-ray attenuation[37,38] and can predict pathological subtypes at specific energies.[39]

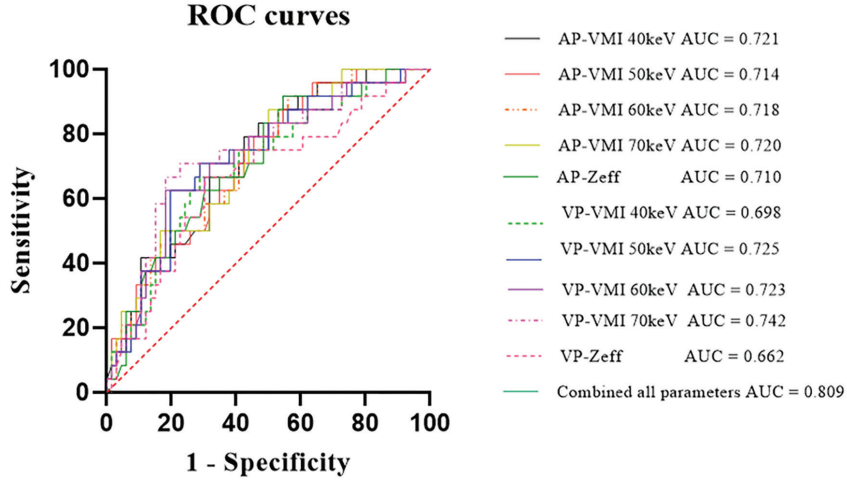

Figure 5. Receiver operating characteristic curves (ROCs) of peritumoral fat spectral parameters for tumor budding grade evaluation in colorectal adenocarcinoma. AUC, area under curve; AP, arterial phase; VP, venous phase; VMI, virtual monoenergetic image.

In our study, VMIs at 40, 50, 60, and 70 keV, Z_{eff} in both AP and VP, and NIC in the VP of peritumoral fat were significantly different between the low-grade TB and intermediate- to high-grade TB groups. This phenomenon likely results from improved visualization of contrast-enhanced lesions at lower VMI energy levels.[40-42] In our cohort, no significant correlations were found between tumor spectral parameters and TB grade, whereas peritumoral fat parameters showed strong associations. This spatial heterogeneity indicates distinct microenvironmental influences on spectral CT parameters. Our findings differ from those reported by Shao et al.,[17] potentially due to divergent DLSCT protocols. Our AP scan was initiated 5 seconds after aortic enhancement reached 150 HU, potentially capturing a later, mixed AP/portal VP phase.

In contrast, Shao et al. triggered scanning immediately upon detection of 100 HU. This fundamental difference in temporal triggering could result in divergent enhancement patterns of both tumor and peritumoral fat, affecting absolute parameter values and their correlation with TB. This likely accounts for the discrepancies in VP characterization observed between the studies.

In the present study, we found that some new parameters are associated with the TB grade in CRAC. Peritumoral fat spectral parameters were not reported in previous studies to predict TB grade in CRAC. In the logistic regression analysis, VMIs at 40, 50, 60, and 70 keV, Z_{eff} in both AP and VP, and NIC in the VP of peritumoral fat were independent predictors of the TB grade in CRAC. We propose that the TB-spectral CT correlation stems from a structural–functional cascade in peritumoral fat. The increase in both VMI attenuation and Z_{eff} can be attributed to several concurrent pathological processes in the peritumoral fat: fibrosis (with higher cellularity and connective tissue deposition), microvascular proliferation (increasing local blood volume), and inflammatory infiltration. These elements have intrinsically higher atomic numbers and density than pure adipose tissue. In parallel, a rise in NIC is a direct biomarker of increased iodine accumulation, signifying enhanced vascular perfusion, and potentially increased vascular permeability, likely mediated by tumor-derived angiogenic signaling. This architectural alteration directly alters X-ray absorption, producing measurable changes in spectral CT parameters, such as attenuation values and spectral λHU.[43]

Consequently, a clinically relevant workflow may be seamlessly integrated into preoperative DLSCT staging, including performing quantitative peritumoral fat analysis, appending the results (e.g., high-grade TB probability) to the radiology report, and thereby informing the multidisciplinary team. This could impact surgical planning (e.g., margin consideration), neoadjuvant therapy stratification in rectal cancer, and postoperative prognostic stratification—especially crucial in stage II colon cancer, where TB is a high-risk feature—guiding follow-up intensity and adjuvant therapy.

This study has some limitations. First, its single-center, retrospective nature, coupled with its limited sample size, may have introduced selection bias. Moreover, the absence of internal validation (e.g., bootstrapping or cross-validation) for the logistic model necessitates future verification in larger, multicenter cohorts. Second, the study focused solely on adenocarcinomas, excluding other CRC histological variants, thereby limiting the applicability of our findings to all CRC subtypes. Third, subgroup distribution was uneven. Fourth, this study did not retrospectively collect body mass index or quantify visceral fat area. Finally, this study was restricted to a single CT vendor's technology, and key parameters (VMI, IC, Z_{eff}) vary across different systems. Therefore, although the diagnostic concept is transferable, our specific thresholds are vendor sensitive, mandating multicenter studies across diverse platforms to derive generalizable standards. Future studies should also explore spectral CT's role in evaluating tumor deposits, undertake multicenter investigations with larger sample sizes to confirm the robustness and reproducibility of these observations, and incorporate DLSCT spectral parameters into machine learning or radiomics models for automated, high-throughput analysis.

In conclusion, DLSCT-derived quantitative parameters of peritumoral fat, particularly VMI and Z_{eff} values from both AP and VP, serve as independent predictors of TB grade in CRAC.

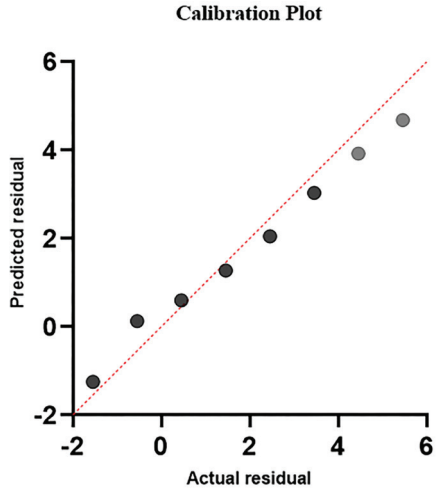

Figure 6. Calibration plot of the final combined logistic regression model.

Variable	OR(95%CI)	*P* value
AP-VMI 40keV	1.026 (0.933 - 1.141)	0.001
AP-VMI 50keV	0.990 (0.786 - 1.195)	0.002
AP-VMI 60keV	0.849 (0.621 - 0.997)	0.002
AP-VMI 70keV	1.157 (0.967 - 1.508)	0.002
AP-Zeff	6.811 (0.016 - 3071)	0.002
VP-VMI 40keV	0.913 (0.963 - 1.444)	0.004
VP-VMI 50keV	1.091 (0.608 - 0.841)	0.001
VP-VMI 60keV	1.062 (0.858 - 1.298)	0.001
VP-VMI 70keV	1.016 (0.897 - 1.131)	0.001
VP-Zeff	0.466 (0.008 - 12.87)	0.019

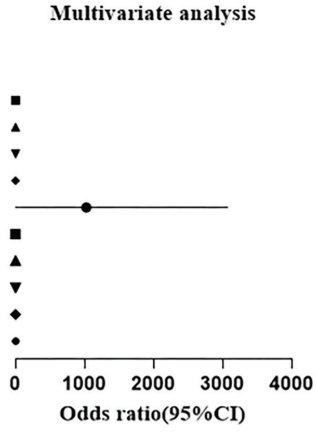

Figure 7. Forest plot of odds ratios from multivariable logistic regression of peritumoral fat. OR, odds ratio; CI, confidence interval; AP, arterial phase; VP, venous phase.

Footnotes

Conflict of interest disclosure

This study was supported by grants from the National Natural Science Foundation of China (No. 82471567, 81801757), Guangdong Basic and Applied Basic Research Foundation (No. 2024A1515010279, 2023A1515010256).

Supplementary: https://d2v96fxpocvxx.cloudfront.net/b65011c5-47cb-4d06-b7cc-d78a7e40a205/content-images/946a7c82-b1e4-4c07-9a2c-20174dc48e34.pdf

References

1. Siegel RL, Miller KD, Wagle NS, Jemal A. Cancer statistics, 2023. *CA Cancer J Clin*. 2023;73(1):17-48. [Crossref]
2. Siegel RL, Wagle NS, Cercek A, Smith RA, Jemal A. Colorectal cancer statistics, 2023. *CA Cancer J Clin*. 2023;73:233-254. [Crossref]

3. Benson AB, Venook AP, Adam M, et al. Colon Cancer, Version 3.2024, NCCN Clinical Practice Guidelines in Oncology. *J Natl Compr Canc Netw*. 2024;22:e240029. [Crossref]
4. Kamall GH, Ulusoy C, Nikolovski A, Kamall S. Tumour budding - an additional prognostic factor in colorectal cancer survival. *Pol J Pathol*. 2023;74:36-41. [Crossref]
5. Basile D, Broudin C, Emile JF, et al. Tumor budding is an independent prognostic factor in stage III colon cancer patients: a post-hoc analysis of the IDEA-France phase III trial (PRODIGE-GERCOR). *Ann Oncol*. 2022;33(6):628-637. [Crossref]
6. Kijima S, Sasaki T, Nagata K, Utano K, Lefor AT, & Sugimoto H. Kijima S, Sasaki T, Nagata K, Utano K, Lefor AT, Sugimoto H. Preoperative evaluation of colorectal cancer using CT colonography, MRI, and PET/CT. *World J Gastroenterol*. 2014;20(45):16964-16975. [Crossref]
7. Zhou XC, Chen QL, Huang CQ, Liao HL, Ren CY, He QS. The clinical application value of multi-slice spiral CT enhanced scans combined with multiplanar reformations images in preoperative T staging of rectal cancer. *Medicine (Baltimore)*. 2019;98:e16374. [Crossref]
8. Inamdar A, Shinde RK. The diagnostic impact of contrast-enhanced computed tomography (CECT) in evaluating lymph node involvement in colorectal cancer: a comprehensive review. *Cureus*. 2024;16:e61832. [Crossref]
9. Li M, Qin H, Yu X, et al. Preoperative prediction of Lauren classification in gastric cancer: a radiomics model based on dual-energy CT iodine map. *Insights Imaging*. 2023;14(1):125. [Crossref]
10. You Y, Wang Y, Yu X, et al. Prediction of lymph node metastasis in advanced gastric adenocarcinoma based on dual-energy CT radiomics: focus on the features of lymph nodes with a short axis diameter ≥6 mm. *Front Oncol*. 2024;14:1369051. [Crossref]
11. Zhu Y, Wang P, Wang B, et al. Dual-layer spectral-detector CT for predicting microsatellite instability status and prognosis in locally advanced gastric cancer. *Insights Imaging*. 2023;14(1):151. [Crossref]
12. Chen W, Ye Y, Zhang D, et al. Utility of dual-layer spectral-detector CT imaging for predicting pathological tumor stages and histologic grades of colorectal adenocarcinoma. *Front Oncology* 2022;12:1002592. [Crossref]
13. Sun Q, Bian X, Sun D, et al. The value of preoperative diagnosis of colorectal adenocarcinoma pathological T staging based on dual-layer spectral-detector computed tomography extracellular volume fraction: a preliminary study. *Jpn J Radiol*. 2024;42:612-621. [Crossref]
14. Lu W, Tan X, Zhong Y, et al. Spectral CT in the evaluation of perineural invasion status in rectal cancer. *Jpn J Radiol*. 2024;42:1012-1020. [Crossref]
15. Yuan X, Quan X, Che X, et al. Preoperative prediction of the lymphovascular tumor thrombus of colorectal cancer with the iodine concentrations from dual-energy spectral CT. BMC Med Imaging. 2023;23(1):103. [Crossref]
16. Chen J, Ni L, Gong J, et al. Quantitative parameters of dual-layer spectral detector computed tomography for evaluating differentiation grade and lymphovascular and perineural invasion in colorectal adenocarcinoma. *Eur J Radiol*. 2024;178:111594. [Crossref]
17. Shao C, He C, Zheng P, Zhou P, Chen X. Preoperative prediction of tumor budding and lymphovascular invasion in colon cancer using dual-energy CT: a prospective study with internal model validation. *Abdom Radiol (NY)*. 2025;50(8):3406-3414. [Crossref]
18. Sun Q, Bian X, Feng F, Chen S, Chen G. A nomogram based on dual-layer spectral detector CT-derived 40KeV virtual monoenergetic images for preoperative prediction of simultaneous distant metastasis in colorectal cancer. *BMC Med Imaging*. 2025;25(1):455. [Crossref]
19. Chen W, Jia Z, Wan L, et al. Interpretable radiomics model based on dual-layer spectral CT iodine maps for predicting microsatellite instability in colorectal cancer: a two-center study. *Eur J Radiol*. 2025;192:112357. [Crossref]
20. Conti G, Calderan L, Quintero Sierra LA, et al. Tumor and peritumoral adipose tissue crosstalk: de-differentiated adipocytes influence spread of colon carcinoma cells. *Tissue Cell*. 2023;80:101990. [Crossref]
21. Amor S, Iglesias-de la Cruz MC, Ferrero E, et al. Peritumoral adipose tissue as a source of inflammatory and angiogenic factors in colorectal cancer. *Int J Colorectal Dis*. 2016;31:365-375. [Crossref]
22. Zoico E, Rizzatti V, Darra E, et al. Morphological and functional changes in the peritumoral adipose tissue of colorectal cancer patients. *Obesity (Silver Spring.)* 2017; 25(Suppl 2):S87-S94. [Crossref]
23. Liesenfeld DB, Grapov D, Fahrmann JF, et al. Metabolomics and transcriptomics identify pathway differences between visceral and subcutaneous adipose tissue in colorectal cancer patients: the ColoCare study. *Am J Clin Nutr*. 2015;102:433-443. [Crossref]
24. Conti G, Minicozzi A, Merigo F, et al. Morphogenetic events in the perinodal connective tissue in a metastatic cancer model. Biomed Pharmacother. 2013;67:1-6. [Crossref]
25. Ahn H, Won Lee J, Jang SH, et al. Prognostic significance of imaging features of peritumoral adipose tissue in FDG PET/CT of patients with colorectal cancer. *Eur J Radiol*. 2021;145:110047. [Crossref]
26. Lugli A, Kirsch R, Ajioka Y, et al. Recommendations for reporting tumor budding in colorectal cancer based on the International Tumor Budding Consensus Conference (ITBCC) 2016. *Mod Pathol*. 2017;30(9):1299-1311. [Crossref]
27. Pesapane A, Capasso L, Del Sorbo MR, et al. Adipose-tumor crosstalk in colorectal cancer: Identifying (Epi)genetic biomarkers for tumor progression and cachexia. *Cell Death Dis*. 2025;16(1):675. [Crossref]
28. Yingying L, Zhe Z, Xiaochen W, Xiaomei L, Nan J, Shengjun S. Dual-layer detector spectral CT-a new supplementary method for preoperative evaluation of glioma. *Eur J Radiol*. 2021;138:109649. [Crossref]
29. Li YX, Li WJ, Xu YS, et al. Clinical application of dual-layer spectral CT multi-parameter feature to predict microvascular invasion in hepatocellular carcinoma. *Clin Hemorheol Microcirc*. 2024;88:97-113. [Crossref]
30. Zhang K, Zhang J, Li M, Liu X, Xu Y. Prediction of histologic grade of hepatocellular carcinoma using dual-layer spectral-detector computed tomography (CT): comparison of two region of interest plotting methods. *Quant Imaging Med Surg*. 2024;14(6):3887-3900. [Crossref]
31. Luo M, Chen G, Xie H, et al. Correction: Preoperative diagnosis of metastatic lymph nodes by CT-histopathologic matching analysis in gastric adenocarcinoma using dual-layer spectral detector CT. *Eur Radiol*. 2023;33(12):9480. Erratum for: Eur Radiol. 2023;33(12):8948-8956. [Crossref]
32. Xu YK, Chai TT, Wang JW, et al. Optimal virtual monochromatic images for assessing metastatic lateral cervical lymph nodes in patients with papillary thyroid carcinoma using duallayer spectral detector computed tomography. *Eur J Radiol*. 2024;178:111623. [Crossref]
33. Wu L, Cen C, Yue X, et al. A clinical-radiomics nomogram based on dual-layer spectral detector CT to predict cancer stage in pancreatic ductal adenocarcinoma. *Cancer Imaging*. 2024;24(1):55. [Crossref]
34. Kim N, Bae K, Kim HC, Jeon KN. Added value of 40 keV virtual monoenergetic images for diagnosing malignant pleural effusion on chest CT. Jpn J Radiol. 2024;42(8):862-871. [Crossref]
35. Zhao L, Zhou W, Fu Y, et al. Diagnostic value of one-stop CT energy spectrum and perfusion for angiogenesis in colon and rectum cancer. *BMC Med Imaging*. 2024;24:116. [Crossref]
36. Sun H, Xu Y, Yang Q, Wang W. Assessment of tumor grade and angiogenesis in colorectal cancer: whole-volume perfusion CT. *Acad Radiol*. 2014;21:750-757. [Crossref]
37. Drljevic-Nielsen A, Donskov F, Mains JR, et al. Prognostic utility of parameters derived from pretreatment dual-layer spectral-detector CT in patients with metastatic renal cell carcinoma. *AJR. Am J Roentgenol*. 2022;218(5):867-876. [Crossref]

38. Garcia LI, Azorin JF, Almansa JF. A new method to measure electron density and effective atomic number using dual-energy CT images. *Phys Med Biol*. 2016;61(1):265-279. [Crossref]

39. Zhu Y, Feng B, Cai W, et al. Prediction of microvascular invasion in solitary AFP-negative hepatocellular carcinoma ≤ 5 cm using a combination of imaging features and quantitative dual-layer spectral-detector CT parameters. *Acad Radiol.* 2023;30(Suppl 1):S104-S116. [Crossref]

40. Liang H, Zhou Y, Zheng Q, et al. Dual-energy CT with virtual monoenergetic images and iodine maps improves tumor conspicuity in patients with pancreatic ductal adenocarcinoma. *Insights Imaging* 2022;13(1):153. [Crossref]

41. Noda Y, Takai Y, Suto T, et al. Effect of X-ray tube on image quality and pancreatic ductal adenocarcinoma conspicuity in pancreatic protocol dual-energy CT. *Clin Radiol.* 2024;79:e554-e559. [Crossref]

42. Woeltjen MM, Niehoff JH, Roggel R, et al. Pancreatic cancer in photon-counting CT: low keV virtual monoenergetic images improve tumor conspicuity. *Eur J Radiol.* 2024;173:111374. [Crossref]

43. Mehta A, Goswami M, Sinha R, Dogra A. Histopathological significance and prognostic impact of tumor budding in colorectal cancer. *Asian Pac J Cancer Prev*. 2018;19(9):2447-2453. [Crossref]